Modeling the zeta potential of silica capillaries in relation to the background electrolyte composition

Claudio L. A. Berli,[1,2] María V. Piaggio [3] and Julio A. Deiber [1]

[1] Instituto de Desarrollo Tecnológico para la Industria Química - Universidad Nacional del Litoral (UNL) - Consejo Nacional de Investigaciones Científicas y Técnicas, Güemes 3450, 3000, Santa Fe, Argentina

[2] Departamento de Física, Facultad de Bioquímica y Ciencias Biológicas (FBCB), UNL, Pje. El Pozo, 3000, Santa Fe, Argentina

[3] Cátedra de Bioquímica Básica de Macromoléculas, FBCB, UNL, Pje. El Pozo, 3000, Santa Fe, Argentina

Shortened version of the title:

Modeling the zeta potential of silica capillaries

Corresponding author:

Julio A. Deiber, INTEC, Güemes 3450, 3000, Santa Fe, Argentina

E-mail: treoflu@ceride.gov.ar

Fax: 0054 - (0)342 – 4550944

List of Abbreviations:

BGE: background electrolyte; CZE: capillary zone electrophoresis; EOF: electroosmotic flow

Keywords: zeta potential, surface charge, background electrolyte, electroosmotic flow, capillary zone electrophoresis.

Summary

A theoretical relation between the zeta potential of silica capillaries and the composition of the background electrolyte (BGE) is presented in order to be used in capillary zone electrophoresis (CZE). This relation is derived on the basis of Poisson-Boltzmann equation and considering the equilibrium dissociation of silanol groups at the capillary wall as the mechanism of charge generation. Therefore, the resulting model involves the relevant physicochemical parameters of the BGE-capillary interface. Special attention is centered in the characterization of the BGE, which can be either salt or/and buffer solutions. The model is successfully applied to electroosmotic flow (EOF) experimental data of different aqueous solutions, covering a wide range of pH and ionic strength. Numerical predictions are also presented showing the capability of the model to quantify the EOF, the control of which is relevant to improve analyte separation performance in CZE.

1 Introduction

The use of capillary electrophoresis for analytic purposes has increased substantially in the last decade. At present, modern and full automatic apparatuses are available allowing separations of analytes in a few minutes. In particular, the method has become a key tool in the analysis of proteins [1] and DNA [2]. Capillary zone electrophoresis (CZE) is one of the separation modes most commonly used in capillary electrophoresis, mainly because the magnitude of the electroosmotic flow (EOF) can be manipulated to optimize the separation performance through appropriate changes of applied electrical field *E*, capillary zeta potential ζ and electrical permittivity to viscosity ratio ε/μ of the background electrolyte (BGE). Other advantages are well-described elsewhere [3-7]. In this sense, two fundamental factors affecting the zeta potential, and hence the EOF, need to be carefully controlled: the charge density on the capillary wall and the chemical composition of the BGE. For this purpose one requires a rational formulation of solutions concerning pH, ionic strength, viscosity and electrical permittivity [7-11]). Frequently the most effective means to control the capillary surface potential consists in modifying pH and ionic strength of the BGE (see also [12] and references therein for a discussion on this aspect). In addition, it is known in practice that the appropriate preparation of the capillary (activation and washing protocols) before the electrophoretic run is a crucial step in separation procedures [9,13].

The separation principle of CZE is based on the electrophoretic mobility, which depends on the ratio between electrical (charge) and friction (shape and size) forces acting on each analyte. Since in most cases analytes move along the tube toward the detector with an effective velocity that is the result of composing the EOF and the electrophoretic migration, the zeta potential must be quantified in order to determine the

absolute particle mobility and other associated properties for a given BGE. Apart from this experimental situation, simulation models of CZE are currently used in laboratories [14] mainly to design and optimize protocols of separation (see [15] for a discussion of different levels of modeling that can supply useful information, and also [16-18] for computational codes predicting the separation of ampholytes). These simulations predict 'virtual electropherograms' on the base of governing equations, which contain relevant physicochemical properties of the capillary, BGE and analytes. Among these properties, the zeta potential is, of course, of particular interest.

To describe and quantify the EOF through the zeta potential, several proposals consist in modeling the electrical double layer with the introduction of parameters like adsorption equilibrium constants of cations, in addition to the number of ionizable groups per unit area of the silica capillary wall n_S and the compact layer thickness d [19,20]. A detailed analysis of ionizable surface group models of aqueous interfaces was carried out by Healy and White [21] where it is evident that several parameters, difficult to estimate experimentally, can emerge when one considers other possible phenomena like cation adsorption at the interface. An equation to evaluate the zeta potential of silica capillaries, and hence the EOF, was also presented by Tavares and McGuffin [12] where the analogy between ion-selective membranes and double layer structure of silica surfaces was considered. In general, one may conclude that theoretical works are still required to find a relation between the zeta potential and the BGE characteristics.

The aim of our work is precisely to derive a theoretical relationship between the zeta potential of silica tubes and the composition of the BGE by including the relevant physicochemical properties of this system. Therefore, a model is developed on the basis of Poisson-Boltzmann equation and considerations of the compact layer adjacent to the surface, which is expressed in terms of an electrical capacitance per unit area. The ion

exchange between surface and BGE, which is the phenomenon determining the EOF, is considered through both the number density n_S and the dissociation constant K_S of the silanol groups attached to the capillary wall. Consequently, this work is organized as follows. General aspects concerning electrokinetic phenomena are considered in Section 2, in particular, the basic equation describing the EOF in capillaries is conceptually discussed. In Section 3, the modeling of the zeta potential of silica capillaries is presented. The framework followed in this section is close to that of Healy and White [21]. The compositions of the BGE used are briefly described in Section 4. Then in Section 5, the model is applied to experimental data taken from the literature as well as to EOF experiments carried out in this work. Concerning this section, one should observe that experimental data involving EOF in capillaries are not readily available in the literature neither easy to process due to the wide diversity of experimental conditions developed in laboratories. For this reason, we use two set of data. One of them [20] considers ζ for a wide range of pH, involving salt solutions as BGE and a rather high capillary diameter. These data have served as relevant illustration of the zeta potential in classical books [5]. The other set (our experimental data) concentrates the study on a typical buffer solution as BGE, covering a pH zone frequently used in practice. Finally in Section 6, the asymptotic responses of the model are discussed and numerical predictions are presented to illustrate the zeta potential under different values of pH and ionic strength.

2 Relation between EOF and capillary zeta potential

In this section we present definitions and fundamental equations that are required in the description of the model proposed here relating the zeta potential of silica capillaries and the BGE composition. Thus, Fig. 1 shows schematically a silica surface associated

with a capillary of length L and radius R in equilibrium with an aqueous electrolyte solution. In this work, for practical reasons to be visualized below, the radial cylindrical coordinate r is expressed through the coordinate $x = R - r$ measuring the distance from the capillary wall. The silanol groups attached to the capillary wall behave as a weak acid. The dissociation of protons generates a negatively charged interface, with charge density per unit area σ_0, and consequently, a surface potential ψ_0. In thermal equilibrium, the distribution of counterions and coions near the interface is given by the balance between entropic and electrostatic forces. In particular, the region between $0 \le x \le d$, the so-called compact layer, is generally assumed to be free of charges due to the finite size of the hydrated ions. Indeed, the magnitude of d is of the order of several angstroms [22]. The surface at $x = d$, also designated the outer Helmholtz plane, involves the potential ψ_d. It is assumed throughout this work that $\zeta \approx \psi_d$ (see also [22,23]). For $x \ge d$, in the diffuse layer, the relationship between the electrostatic potential $\psi(x)$ and the ion densities is governed by Poisson-Boltzmann equation,

$$\frac{1}{(x+R)^n}\frac{d}{dx}\left((x+R)^n \frac{d\psi}{dx}\right) = -\frac{e}{\varepsilon}\sum_k z_k n_k^b \exp\left(-\frac{e z_k \psi}{k_B T}\right) \qquad (1)$$

with boundary conditions $\psi|_{x=d} = \zeta$ and $\left.\frac{d\psi}{dx}\right|_{x=R} = 0$. In Eq. (1), the parameter n is used to describe either the planar (n=0) or axisymmetric (n=1) geometries [24]. Also, e is the elementary charge, k_B is the Boltzmann constant, z_k are the ion valences, T is the absolute temperature and n_k^b are the ion densities in the solution bulk. In fact, as shown in Fig. 1b, $\psi(x)$ decreases away from the plane at $x = d$ and may tend to a value different from zero at the capillary center line [24], depending this response on the relative value of the zeta potential and the ionic strength of the BGE. For later use we

also define the parameter $\kappa = \left(2e^2 I\ N_{\mathrm{A}} 10^3 / \varepsilon k_{\mathrm{B}} T\right)^{1/2}$, which is equal to the inverse of the Debye length λ. In this equation, $I = \frac{1}{2}\sum_k z_k^2 c_k$ is the ionic strength, where $c_k = n_k^b / 10^3 N_{\mathrm{A}}$ are molar concentrations and N_{A} is the Avogadro number. When an electrical field is applied along the capillary (normal to the *x*-direction in Fig. 1) the electric force acting on the ions moves them in the field direction, dragging the BGE through the capillary. Hence the electroosmotic velocity profile $v(x)$ develops as pictured in Fig. 1c.

Recently, Griffiths and Nilson [24] (see also [25]) carried out numerical solutions of Eq. (1) coupled to the species balance and to the Navier-Stokes equation involving the electrical force, in order to obtain the electrical potential, fluid velocity and late-time solute distribution for the electroosmotic flow in a tube and channel at zeta potentials not necessarily small. From this study it becomes evident that the effect caused on the electroosmotic velocity and electrical potential profiles by increasing the dimensionless number $ez_k\zeta / k_B T$ is analogous to that obtained by decreasing the ratio λ / R, where $\lambda = 1/\kappa$. Thus, for intermediate values of the zeta potential typically found in CZE and when $\lambda / R << 1$, one may attain a near plug EOF, viz. the Hemlholtz-Smoluchowsky relation applies. In fact, Gaš et al. [26] clearly demonstrated this conclusion pertaining to the EOF in CZE on the base that the electrical potential around the center of the capillary is near zero in electrophoretic columns with diameters above 10 μm. This flow situation is achieved because the variation of $\psi(x)$ is confined within the small region $d \le x \le \lambda$, provided the Joule effect associated with the electrical current has been appropriately minimized. For example, values like pH 9, $I \approx 10$ mM and $2R \approx 75$ μm yield $\lambda / R \approx 10^{-4}$, which is a value small enough to consider $\psi|_{x=R} \approx 0$. Since in typical runs of CZE this condition is fully satisfied, the curvature of the tube may be neglected

in Eq. (1) for the purposes of calculating ζ by putting $n = 0$. Despite the above considerations of the EOF in CZE, one should observe that after neglecting the capillary curvature and consequently taking the electrical potential asymptotically null at the capillary center line, the nonlinear response of Poisson-Boltzmann equation is still considered fully in our analysis. Thus, Eq. (1) with $n = 0$ gives results valid for high values of ζ, i.e., the Debye-Hückel approximation is not applied.

From the kinematic point of view, the relation between the EOF and the zeta potential in capillaries has received special attention in the literature during the last years, mainly to visualize under which physicochemical conditions classical hypothesis are valid to yield, for instance, the Helmholtz –Smoluchowski relation for a near plug electroosmotic velocity (see, for example, [24,26,27]). The motivation of these studies responds in part to the earlier result reported by Rice and Whitehead [28] indicating that stationary velocity profiles of the EOF in cylindrical capillaries calculated through a linear approximation of the exponential terms in the Poisson-Boltzmann equation fails when the absolute value of the zeta potential becomes higher than around 50 mV (see also [29,30] where this subject is considered in relation to liquid chromatography). These results clearly indicated that numerical solutions might be required to evaluate precisely the different physical situations under which the EOF was developed and, in addition, to understand how these situations were related to the practice of CZE. Important studies in this aspect are [26,27] where profiles of the electrical potential in the diffuse layer are calculated from the Poisson-Bolztmann equation expressed in the cylindrical coordinate system without any approximation. In these works, it is also possible to find an analytic expression for the electroosmotic velocity profile in terms of the electrical potential of the diffuse layer under isothermal conditions of the BGE, as follows:

$$v(x) = -\frac{\varepsilon E \zeta}{\mu}\left(1 - \frac{\psi(x)}{\zeta}\right) \tag{2}$$

Within the same context of analysis of Eq. (2) and including the energy balance of the BGE [31,32], it is reported [14] that under nonisothermal conditions, the axial electroosmotic velocity $v(x)$ may be expressed through Eq. (2) plus a term of the order of the Grashof number $N_{\mathrm{Gr}} = \frac{3\rho\beta\alpha E R^4}{64\varepsilon k \zeta}$, which is negligible for small capillary radius. In this dimensionless number, β is the thermal expansion coefficient, α is the electrical conductivity and *k* is the thermal conductivity, all of the BGE. In fact, the value of N_{Gr} measures the distortion of the EOF provided by Eq. (2), when thermal effects become important. For $N_{\mathrm{Gr}} \to 0$, the result found in [14] is consistent with Eq. (2). It is also observed in Eq. (2) that the fluid velocity vanishes at $x = d$ satisfying the classical non-slip boundary condition. In addition, as λ/R is small in CZE, the potential vanishes for $x >> \lambda$ and the fluid velocity reaches the limiting near plug value v_{EO}. When all the above conditions are satisfied, one obtains [26],

$$v_{EO} \approx -\frac{\varepsilon E \zeta}{\mu} \tag{3}$$

which is the Helmholtz-Smoluchowski equation relating ζ to the EOF velocity. From Eq. (3), v_{EO} can be determined experimentally by using neutral markers, which move along the capillary due to the EOF only. Therefore, the electroosmotic velocity can be evaluated with $v_{\mathrm{EO}} \approx L_d / t_m$, where L_d is the capillary detection length and t_m is the marker migration time.

3 Modeling the capillary zeta potential

3.1 Concepts associated with charged interfaces

In this section several concepts required to study a charged interface in equilibrium with an aqueous electrolyte solution are presented. The surface charge density σ_0, generated by the dissociation of silanol groups on the capillary wall, is balanced with the total charge in the diffuse layer of ions, σ_d. Therefore, the electroneutrality of the system is established through,

$$\sigma_d + \sigma_0 = 0 \tag{4}$$

where,

$$\sigma_d = \int_R^d e\sum_k z_k n_k^b \exp\left(-\frac{ez_k\psi}{k_{\mathrm{B}}T}\right)dx \tag{5}$$

Combining Eq. (1) with $n = 0$ and Eq. (5), and considering boundary conditions, one obtains,

$$\sigma_d = \left\{2\varepsilon k_B T \sum_k n_k^b\left[\exp\left(-\frac{ez_k\zeta}{k_{\mathrm{B}}T}\right)-1\right]\right\}^{1/2} \tag{6}$$

This equation, also named the Grahamme equation, provides a relationship between the surface charge and the concentration of ions in solution. For the particular case of a symmetric electrolyte ($z_+ = -z_- = z$) in equilibrium with an infinitely large reservoir ($n_+^b = n_-^b = n^b$), Eq. (6) gives the result of the Gouy-Chapman model expressed [32],

$$\sigma_d = -\left(8\varepsilon k_B T\, n^b\right)^{1/2}\sinh\left(ze\zeta/2k_B T\right) \tag{7}$$

The above assumptions also imply that the concentration of counterions neutralizing the surface charge of the capillary wall is negligible in comparison with the concentration of electrolyte ions in the bulk.

On the other hand, the potential in the compact layer requires different physical considerations. In order to simplify calculations, a common practice in the literature is to interpret the equi-potential planes at $x = 0$ and $x = d$ as a pair of charged plates

forming a capacitor. Thus, since ions are excluded from this region, the potential drop across the layer $0 \le x \le d$ is assumed to be linear, i.e.,

$$\psi_0 - \zeta = \sigma_0 / C_{in} \tag{8}$$

where C_{in} is the capacitance per unit area of the inner region between these plates [22]. The introduction of C_{in} in the compact layer is required to describe appropriately the relation between ψ_0, which may be evaluated through charge titration, and ζ obtained from measurement of the electroosmotic velocity given by Eq. (3).

3.2 Surface chemistry and surface potential

The surface potential ψ_0 develops after dissociation of silanol groups attached to the silica capillary wall, as mentioned in the previous section (Fig. 1a). This dissociation is represented by the chemical equilibrium,

$$\text{—SiOH} \leftrightarrows \text{—SiO}^- + \text{H}^+$$

similar to that of a weak acid in aqueous solution. In silica tubes, the number of ionizable sites per unit area of the surface is approximately $n_S \sim 10^{17}$ m^{-2} [4,32]. Thus, calculations indicate that the maximum concentration of protons released to the medium is negligible in comparison to typical concentrations of salt used in CZE. This fact greatly simplifies calculations since the amount of H^+ in solution is controlled exclusively by the acid/base added to the BGE. Therefore, the relation between the concentration of protons in the bulk and the surface charge density can be readily established. For this purpose, we consider a system composed of a solid surface containing both species —SiOH and —SiO$^-$ in equilibrium with a large electrolyte reservoir. This reservoir is the electrolyte solution, where the electrostatic potential is $\psi \approx 0$ in the bulk according to previous considerations for small λ / R. Therefore, to

express the equilibrium equation involving the process of dissociation of silanol groups, the chemical potentials of species must include appropriately the electrostatic contribution to the free energy in addition to that pertaining to the entropy of mixing [33]. On the basis of statistical thermodynamics, and assuming that the mixture is ideal (activity coefficients are unity; see also [7] for a discussion on this last aspect), one obtains the equilibrium constant K_S as follows [21]:

$$\frac{[\text{–SiO}^-][\text{H}^+]}{[\text{–SiOH}]} = K_\text{S} \exp\left(e\psi_0 / k_B T\right) \tag{9}$$

where $[\text{–SiO}^-]$ and $[\text{–SiOH}]$ represent surface concentrations expressed in moles/m^2, while $[\text{H}^+]$ stands for the proton concentration in the solution bulk in moles/m^3. The factor $\exp\left(e\psi_0 / k_B T\right)$ can be interpreted as the electrostatic contribution to the energy of the charged surface groups, —SiO$^-$, which are subjected to the surface potential ψ_0. Other authors simply consider that $[\text{H}^+] \exp\left(-e\psi_0 / k_B T\right)$ represents the actual concentration of protons at the solid surface where the dissociation reaction takes place [34]. From Eq. (9), the surface charge is readily found to be,

$$\sigma_0 = \frac{-en_\text{S}}{1 + ([\text{H}^+]/K_\text{S}) \exp\left(-e\psi_0 / k_B T\right)} \tag{10}$$

where en_S is the total number of surface charges available.

3.3 Model and calculation procedure

As stated in the Introduction, we are interested in predicting the zeta potential from the knowledge of the BGE characteristics. For this purpose, we relate Eqs. (4), (8) and (10). Thus, ζ can be determined from the following expression,

$$\sigma_d(n_k^b,\zeta) - \frac{en_S}{1+\left(\frac{[H^+]}{K_S}\right)\exp\left\{\frac{-e}{k_BT}\left[\zeta - \frac{\sigma_d(n_k^b,\zeta)}{C_{in}}\right]\right\}} = 0 \qquad (11)$$

where $\sigma_d(n_k^b,\zeta)$ is given by Eq. (6). In particular, for symmetric electrolytes Eq. (7) may be used. The scope of Eq. (11) is quite general as long as the ion densities are appropriately quantified for each BGE (see Section 4). It should be pointed out here that a simpler expression for the zeta potential has been derived in the literature [21] by assuming $C_{in} \to \infty$, and hence $\psi_0 \approx \zeta$. In addition, it was considered z:z electrolytes only, i.e., $\sigma_d(n_k^b,\zeta)$ was obtained from Eq. (7).

In Eq. (11) one may recognize parameters characterizing the capillary (n_S, K_S, C_{in}), the BGE (n_k^b, [H$^+$]) and the capillary zeta potential (ζ). Provided the composition of the BGE is known from the formulation procedure (Section 4), the first step in our calculations is to evaluate these capillary parameters. A set of *N* experimental data {pH, *I*, ζ} is required for this purpose. Then, n_S, K_S and C_{in} are determined as the values that minimize, for the whole data set, the left hand side of Eq. (11) designated Δ. In this sense, we find the minimum of the sum of squares, $\sum_{i=1}^{N}(\Delta_i)^2$, where the sub-index *i* refers to each triad {pH, *I*, ζ} of experimental data placed into Eq. (11). Numerical calculations were carried out by means of a typical minimizing subroutine based on Newton method. The relative standard deviation of fitting was always less than 5% in all the samples analyzed. Once the parameters of the capillary are known, the zeta potential for a different electrolyte composition can be predicted with the same numerical scheme, where the input data are {pH, *I*} and the only unknown is ζ.

4 Composition of the background electrolyte

To obtain meaningful experimental data of the EOF in fused silica capillaries, the calculation of the ionic strength of different solutions used in the experimental program must be carried out carefully, avoiding rough approximations that usually introduce errors at extreme values of pH and salt concentrations. For this reason, here we mention numerical concerns relevant to the calculations of *I* for the two types of BGE used in this work.

For solutions of 1:1 salts, for instance KNO_3, the ionic strength is simply $I \approx [KNO_3]$, when the contribution from water dissociation is neglected. In EOF experiments, the pH of the solution is varied by adding either KOH or HNO_3. In this process, the ionic strength can be considered constant if the initial concentration of salt, $[KNO_3]$, exceeds largely the concentration of acid or base added to adjust the pH. Otherwise, when salt concentration is rather low, the equivalents of base or acid added have to be considered. Also for this electrolyte solution, the charge density $\sigma_d(n_k^b, \zeta)$ entering Eq. (11) may be evaluated through Eq. (7), in which $n^b \equiv 10^3 N_A I$.

In the case of solutions of $Ba(NO_3)_2$, for example, the contribution of divalent ions to the ionic strength is particularly important. In addition, the pH of the solution is increased with $Ba(OH)_2$ or decreased with HNO_3. Taking into account these contributions, the ionic strength for this case may change significantly for pH values different from around 7. Nevertheless, in the case of a 2:1 electrolyte, the charge density $\sigma_d(n_k^b, \zeta)$ must be evaluated necessarily through Eq. (6), because it cannot be expressed explicitly in terms of *I*.

In CZE determinations and also in the experimental evaluation of the corresponding EOF, the pH of the solution is commonly controlled with an appropriate buffer. Following this practice, in the experiments carried out in this work (Section 5.2), borate

buffer (conjugate $BO_3H_3/BO_3H_2^-$ pair) is used, the pK_a value of which is 9.2 at 25°C. Also a strong base (NaOH) is added to the solution to increase the pH. Therefore, the ionic strength is determined mainly by the equivalents of $BO_3H_2^-$ present in the medium. Nevertheless, for low and high pH values the approximate expression $I \approx c_0/\left(1+10^{-(pH-pK_a)}\right)$, where c_0 is the molar concentration of boric acid used in the solution formulation, must be corrected due to the contribution of $[H^+]$. For further discussions below, the ionic strength versus pH for different values of c_0 is showed in Fig. 2 indicating the range of pH (shaded zone) where the buffering power is maximum.

5 Application of the model to experimental data

5.1 Data involving salt solutions

In this section the model is applied to experimental data of zeta potential as a function of pH when the BGE is a salt solution. Although results and details of the experimental technique are well-described elsewhere [20] it is relevant to point out here that measurements were carried out in a vitreous silica capillary, 760 μm of diameter and 0.30 m of length. Also temperature was 25 °C and hence $\varepsilon = 6.95\ 10^{-10}$ C^2/Nm^2 for the aqueous solution. The parameter values of the model obtained with the data of this work for different electrolyte compositions are reported in Table 1. Figure 3 presents ζ as a function of pH for different concentrations of a 1:1 electrolyte. Symbols indicate experimental results [20] and lines refer to the predictions of the model when the parameter values reported in Table 1 are used. A remarkable agreement between theory and experiments is observed for the whole range of pH and salt concentrations. It is relevant to observe that almost the same numerical values of K_S are obtained for the salt concentrations studied here. In relation to data in Table 1, one should also observe

that typical values of C_{in} are in the range 0.1-1 Fm^{-2} for the case of acid groups attached to solid surfaces [22]. Also the number of ionizable silanol groups found was of the same order of magnitude as that reported typically in the literature [4,32] despite we registered a small change with *I*. This smooth variation of the parameter n_S probably indicates that the effective number of surface charges may change with 1:1 salt concentration.

Figure 4 presents ζ as a function of pH for different concentrations of a 2:1 electrolyte. Again, symbols indicate experimental results [20] and lines refer to the model predictions with parameter values reported in Table 1. It is relevant to point out here that the model predicts appropriately the minimum of ζ as a function of pH. Different explanations were made in the literature in order to interpret this behavior in EOF experiments [20]. Here we found that the curves ζ(pH) are satisfactorily described when the composition of the BGE is evaluated rigorously. In fact, the minimum is predicted by the model only in the case that the equivalents of $Ba(OH)_2$ added to increased the pH are considered in the evaluation of $\sigma_d(n_k^b,\zeta)$. Consistently, the summation over all ion species in Eq. (6) is carried out as follows,

$$\frac{\sum_k n_k^b\left(\mathrm{e}^{-z_k\Psi}-1\right)}{10^3 N_\mathrm{A}} \approx \begin{cases} [\mathrm{Ba(NO_3)_2}]\left(2\mathrm{e}^{\Psi}+\mathrm{e}^{-2\Psi}-3\right)+10^{(\mathrm{pH}-14)}\left(\mathrm{e}^{\Psi}+\mathrm{e}^{-2\Psi}/2-3/2\right), \\ \mathrm{pH}>7; \\ [\mathrm{Ba(NO_3)_2}]\left(2\mathrm{e}^{\Psi}+\mathrm{e}^{-2\Psi}-3\right)+10^{-\mathrm{pH}}\left(\mathrm{e}^{\Psi}+\mathrm{e}^{-\Psi}-2\right), \\ \mathrm{pH}<7. \end{cases}$$

where $\mathrm{e}=\exp(1)$ and $\Psi = e\zeta / k_B T$. Therefore, for pH values higher than 7 approximately, the absolute value of ζ decreases due to an increase of the ionic strength with pH.

5.2 Data involving buffer solutions

5.2.1 Experimental

EOF measurements were made by using a commercial P/ACE 5010 Beckman Instrument (Fullerton, CA, USA). A fused silica capillary 0.47 m of total length and 75 μm of inner diameter was used. The UV detector was placed at 0.40 m from the inlet of the capillary. The applied voltage was 20 kV and the temperature was fixed at 25 °C, which was controlled by the liquid thermostating system. One of the EOF markers used was caffeine (FADA) with a concentration of 250 μg/ml prepared in destilled water. Therefore, hydrodynamic injection of the EOF marker was performed at a pressure difference of 0.5 psig with an injection time of 2 s. The electropherogram was recorded within 4 min by using UV absorbance detector operated at 214 nm. The buffers used were aqueous solutions of boric acid (Sigma), the concentration of which was formulated to keep the ionic strength in the range 2-100 mM. The pH was adjusted in the range $8 \le \mathrm{pH} \le 10$ by adding 10 M NaOH. Also, pH values were controlled with a pH-meter (Orion-410A, Beverly, MA, USA). The capillary tube was activated by washing it during 15 min with HCl 0.1 N, 15 min with H_2O, 30 min with OHNa 0.1 N, 30 min with H_2O and 30 min with the desired borate buffer. Each change of pH and ionic strength of the buffer involved tube washing during 3 min with OHNa 0.1 N, 3 min with H_2O and 5 min with the new buffer solution. At least three runs were made for each one of the determinations and a relative standard deviation less than 0.5% resulted for the values of migration times t_m. Experimental data thus obtained were also cross-checked by using dimethyl sulfoxide (Sigma) at 5% in destilled water as marker, with an injection time of 1 s. Finally, ζ values were calculated with Eq. (3).

5.2.2 Results

Figure 5 presents experimental data obtained for different buffer concentrations. In this figure, lines refer to model prediction with the following parameter values: $\mathrm{p}K_S$ = 6, C_{in} = 1 Fm^{-2} and $n_S = a + b\,c_0$, where a = 2.44 10^{17} m^{-2} and b = 14.6 10^{17} $\mathrm{m}^{-2}\mathrm{M}^{-1}$

for $0.025 \leq c_0 \leq 0.1\ M$. Results show that the pK_S obtained coincides with the value reported elsewhere [35]. Having into account that all these parameters are physically meaningful, one may conclude that the model is able to predict the experimental data of ζ for different paths of pH and *I*. These paths are generated by using the appropriate relations between pH and *I* (see also Section 4) at a specified concentration of buffer c_0.

It is clear from the above results that the values found for the parameters (n_S, K_S, C_{in}) characterizing a fused silica capillary are different from those corresponding to a vitreous silica capillary. In principle, one should observe that different process of fabrication of silica capillaries may yield different values of zeta potentials for a given BGE. In this sense, fused silica capillaries are made by melting the purest forms of naturally occurring silicon dioxide at very high temperatures [4]. In this process, the capillaries are being drawn from the hot bulk material and then quenched and exposed to the moisture of the atmosphere. Then, a slow process of relaxation involving the strained siloxane groups allows the acceptance of hydroxide groups from water, which generates a coverage of silanol groups. Consequently, the value of n_S for a fused silica capillary ($2.8 – 3.5\ 10^{17}$ sites/m^2) is expected to be higher than that of a classical vitreous capillary ($0.43 – 1.27\ 10^{17}$ sites/m^2), which is a result observed in our calculations.

In addition to the above result, it should be pointed out that a definite value of pK_S for silica capillaries is not possible to be specified in general, having into account that for the case of fused silica capillaries, at least five types of surface silanol groups with different chemical environments can be found, depending on the fabrication process (see [4] and references therein). Thus, as suggested by Jandik and Bonn [4], it is probably correct to think that the pK_S values of silica capillaries are in a certain range

rather than at a single definite value. Further, in this context of analysis, one could think that the siloxane groups are predominant in the case of the vitreous silica capillary leading to a lower value of its pK_S in comparison with that of the fused silica capillary.

6 Further prediction of the model

Once the model parameters for a given capillary are known, the model allows one to predict the zeta potential for a different electrolyte composition. More precisely, one can estimate ζ for different values of pH and *I*. As an example, additional calculations of ζ involving the fused silica capillary discussed in Fig. 5 are presented in Fig. 6. In this figure, the shaded zone indicates the pH range where the model is compared with experimental data of our work (see also Figs. 2 and 5). This zone is precisely where boric acid has its effective buffering action. Out of this zone, the model prediction is consistent with the expected response of ζ as a function of pH and ionic strength. In particular, one can visualize in this figure that the point of zero charge at pH around 2.5 is predicted, in coincidence with results reported in previous experimental works [20,22]. One concludes that through these extrapolations, the model is useful to formulate properly the BGE in order to obtain a well-defined zeta potential in CZE experiments.

Figure 7 shows another relevant example of the model prediction. In fact, numerical calculations of ζ(pH) are presented when different concentrations of a 1:1 salt is added to the buffer solution. It is observed that the zeta potential curve changes substantially in shape when the salt concentration is increased to a value of 150 mM and, as expected, the curve shifts to lower potentials. In particular, this curve gets a plateau for $9 \leq \text{pH} \leq 12$. This example clearly illustrates that the intensity of the EOF has in general a rather complex response in terms of pH and *I*.

Finally, it is also worth to mention that the asymptotic prediction of the model for the case $C_{in} \to \infty$ was also studied here by using the experimental data of our work. In this sense, although qualitative trends are still acceptable, the quantitative results (not shown here) fails mainly for solutions of 2:1 electrolytes.

7 Concluding remarks

The model developed in this work to quantify the EOF in CZE is composed of two fundamental equations. One provides the diffuse layer charge obtained from Poisson-Boltzmann equation (Grahamme equation in general, or the Gouy-Chapman model for z:z electrolytes in particular). The other models the surface charge with three basic parameters: the number density n_S of silanol groups at the capillary wall, the dissociation constant K_S of these groups and the electrical capacitance of the compact layer C_{in}. The zeta potential is obtained from an implicit function involving pH and *I*, which results by equating these two basic equations. The model predicts well experimental data for different BGE, mainly for complex paths involving changes of pH and ionic strength. In particular, the model indicates that the absolute value of ζ decreases with pH due to an increase of the ionic strength with the equivalent of base added. This effect is evident for pH values higher than 7. Thus, in principle, it should not be necessary to look for further complex phenomena in order to understand this behavior of ζ in terms of pH and *I*, which can be effectively described through a physically meaningful model like the one proposed in this work. In this sense, computational algorithms used to design and optimize the method development of analyte separations in CZE can be benefited from these results.

Authors wish to thank the financial aid received from the Secretaría de Ciencia y Técnica, Universidad Nacional del Litoral, Argentina (CAI+D 2002) and SEPCYT-FONCYT (PICT 09-09752).

8 References

[1] Dolnik, V., *Electrophoresis* 1999, *20*, 3106-3115.

[2] Righetti, P. G., Gelfi, C., D'Acunto, M. R., *Electrophoresis* 2002, *23*, 1361-1374.

[3] Grossman, P. D., Colburn, J. C. (Eds.), *Capillary Electrophoresis: Theory and Practice*. Academic Press, New York 1992, pp. 3-43.

[4] Jandik, P., Bonn, G., *Capillary Electrophoresis of Small Molecules and Ions*. VCH Publishers, New York 1993, pp. 11-31.

[5] Khun, R., Hoffstetter-Khun, S., *Capillary Electrophoresis: Principles and Practice*. Springer-Verlag, Cambridge, UK 1993, pp. 22-29.

[6] Poppe, H., *Advances in Chromatography* 1998, *38*, 233-300.

[7] Kenndler, E., *Chemical Analysis Series* 1998a, *146*, 25-76.

[8] Kenndler, E., Gassner, B., *Anal. Chem.* 1990, *62*, 431-436.

[9] Schwer, Ch., Kenndler, E., *Anal. Chem.* 1991, *63*, 1801-1807.

[10] Kenndler, E., Friedl, W., *J. Chromatogr.* 1992, *608*, 161-170.

[11] Kenndler, E., *J. Microcolumn Separation* 1998b, *10*, 273-279.

[12] Tavares, M. F. M., McGuffin, V. L., *Anal. Chem.* 1995, *67*, 3687-3696.

[13] Lambert, W. J., Middleton, D.L. *Anal. Chem*. 1990, *62*, 1585-1587.

[14] Piaggio, M. V., Deiber, J. A., Proceedings of the *Third Mercosur Congress on Process Systems Engineering and First Mercosur Congress on Chemical Engineering*, Santa Fe, Argentina 2001, III, pp. 1333-1339.

[15] Reijenga, J. C., Kenndler, E., *J. Chromatogr. A* 1994, *659*, 403-415; 417-426.

[16] Mosher, R. A., Dewey, D., Thormann, W. Saville; D. A., Bier, M., *Anal. Chem.* 1989, *61*, 362-366.

[17] Saville, D. A., Palusinski, O. A., *AIChE J.* 1986, *32*, 207-214.

[18] Palusinski, O. A., Graham, A., Mosher,R. A., Bier, M., Saville, D. A., *AIChE J.* 1986, *32*, 215-223.

[19] Salomon, K., Burgi, D. S., Helmer, J. C., *J. Chromatogr*. 1991, *559*, 69-80.

[20] Wiese, G. R.; James, R. O., Healy, T. W., *Discuss. Faraday Soc.* 1971, *52*, 302-311.

[21] Healy, T. W., White, L. R., *Adv.Colloid Interface Sci*. 1978, *9*, 303-345.

[22] Hunter, R. J., *Foundations of Colloid Science*, Vol. II., Clarendon Press, Oxford 1992, pp. 720-756.

[23] Attard, P., Antelmi, D., Larson, I., *Langmuir*, 2000, *16*, 1542-1552.

[24] Griffiths, S. K., Nilson, R. H., *Anal. Chem.* 2000, 72, 4767-4777.

[25] Gross, R. J., Osterle, J. F., *J. Chem. Phys*. 1968, *49*, 228-234.

[26] Gaš, B. Štèdrý, M., Kenndler, E., *J. Chromatogr. A* 1995, 709, 63-68.

[27] Andreev, V. R., Lisin, E. E., *Electrophoresis* 1992, 13, 832-837.

[28] Rice, C. L., Whitehead, R. , J. Phys. Chem. 1965, 69, 4017-4024.

[29] Martin, M., Guiochon, G., *Anal. Chem.* 1984, 56, 614-620.

[30] Martin, M., Guiochon, G.,Walbroehl, Y., Jorgenson, J. W., *Anal. Chem.* 1985, 57, 559-561.

[31] Probstein R. F., *Physicochemical Hydrodynamics*, Butterworths, New York 1989, pp. 185-198.

[32] Russel, W. B., Saville, D. A., Schowalter, W. R., *Colloidal Dispersions*, Cambridge University Press, Cambridge, UK 1989, pp. 96–108.

[33] Evans F. F., Wennerström, H., *The Colloidal Domain*, Wiley-VCH, New York 1999, pp. 127-130.

[34] Gisler, T., Schultz, S. F., Borkovec, M., Sticher, H., Schurtenberger, P., D´Aguanno, B., Klein, R., *J. Chem. Phys.* 1994, *101*, 9924-9936.

[35] Hewlett-Packard Instrument Guide (CD-ROM, Plate 010-023: CE Basics, Fundamental Expressions), 2000.

Table 1. Parameter values of the model obtained in the prediction of EOF data for a vitreous silica capillary.

Electrolyte	Concentration (mM)	pK_S	C_{in} (Fm^{-2})	n_S (10^{17} m^{-2})
KNO_3	0.1	3.51	0.18	1.27
	1		0.17	0.80
	10		0.10	0.35
$Ba(NO_3)_2$	0.033	3.68	0.52	0.42
	0.1			0.45
	0.333			0.43

Figure Captions

Figure 1. (a) Schematic representation of the capillary wall with dissociated silanol groups containing negative electrical charges. The charged surface induces the formation of a diffuse layer of ions in the electrolyte solution. (b) Electrostatic potential $\psi(x)$ as a function of the distance x measured from the charged surface. The Debye length, λ, measures the thickness of the diffuse double layer under typical conditions of CZE. (c) Fluid velocity profile $v(x)$ due to an electric field acting along the capillary. In this figure, d is the thickness of the compact layer, ψ_0 is the surface potential, ψ_d is the potential at the outer Helmholtz plane (it is assumed $\zeta \approx \psi_d$) and v_{EO} is the limiting electroosmotic velocity. The whole diagram emphasizes the solid-liquid interface.

Figure 2. Ionic strength as a function of pH for the buffer $BO_3H_3/BO_3H_2^-$ at 25ºC. The shaded zone shows the range of pH where the buffering power is maximum and where experimental results are reported.

Figure 3. Zeta potential of a vitreous silica capillary as a function of pH, for different concentrations of KNO_3. Symbols are experimental data from Wiese et al. (1971). Lines are the prediction of the model with the parameter values reported in Table 1.

Figure 4. Zeta potential of a vitreous silica capillary as a function of pH, for different concentrations of $Ba(NO_3)_2$. Symbols are experimental data from Wiese et al. (1971). Lines are the prediction of the model with the parameter values reported in Table 1.

Figure 5. Zeta potential of a fused silica capillary as a function of pH, for different concentrations of BO_3H_3 (buffer). Symbols are experimental data obtained in this work. Lines are the predictions of the model with the following parameter values: $pK_S = 6$, $C_{in} = 1$ Fm^{-2} and $n_S = a + b\,c_0$, with $a = 2.44\ 10^{17}$ m^{-2} and $b = 14.6\ 10^{17}$ m^{-2} M^{-1}.

Figure 6. Zeta potential predicted by the model in a wide range of pH. The BGE is the boric buffer solution at different concentrations. The parameter values used in calculations are those reported in Fig. 5.

Figure 7. Zeta potential predicted by the model in a wide range of pH. The BGE is composed of BO_3H_3 50 mM (buffer) and different concentrations of a z:z salt (NaCl). The parameter values used in calculations are those reported in Fig. 5.

Figure 1

Berli, Piaggio and Deiber, 2002.

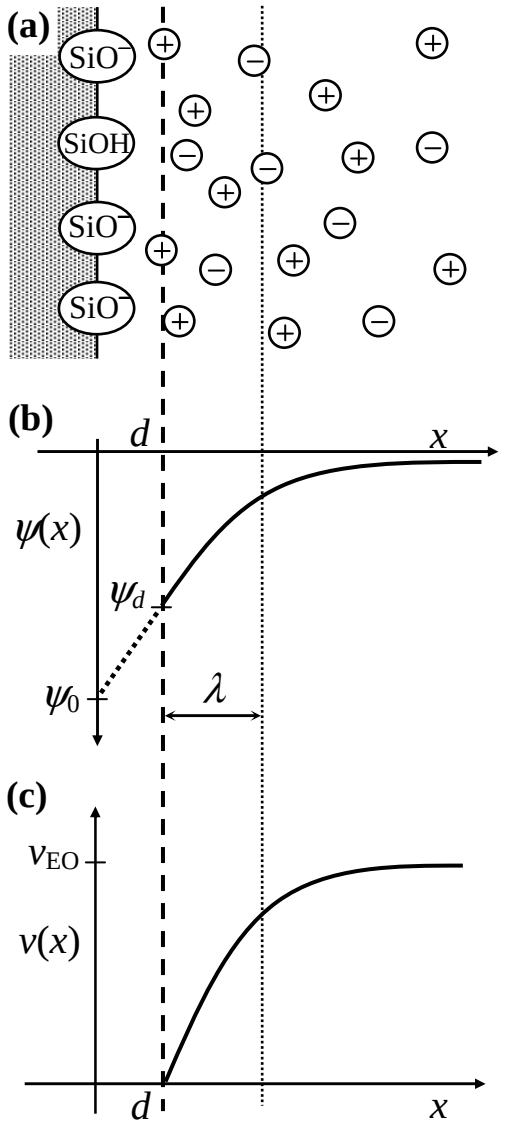

Figure 2

Berli, Piaggio and Deiber, 2002.

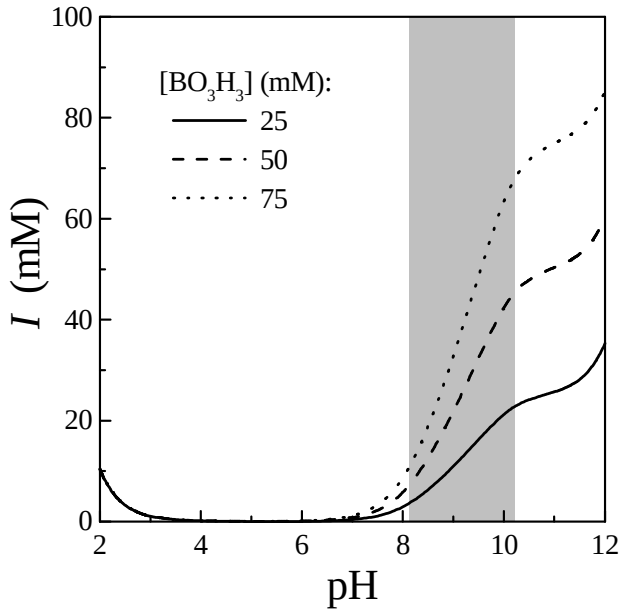

Figure 3

Berli, Piaggio and Deiber, 2002.

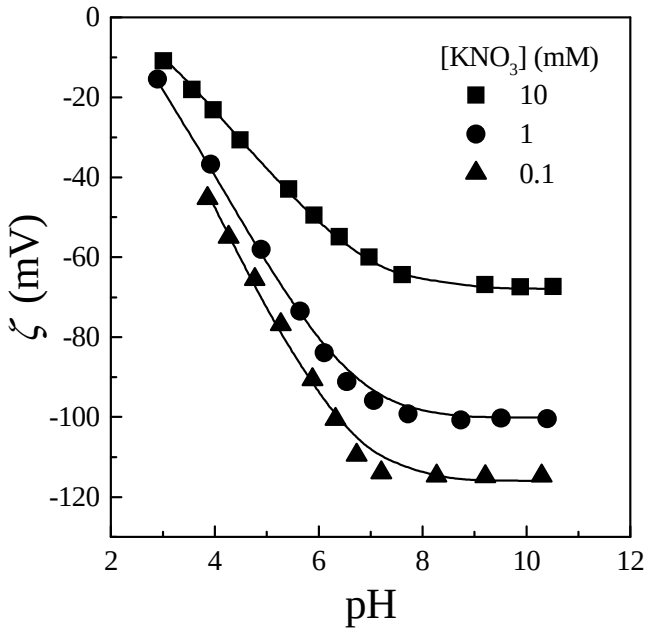

Figure 4

Berli, Piaggio and Deiber, 2002.

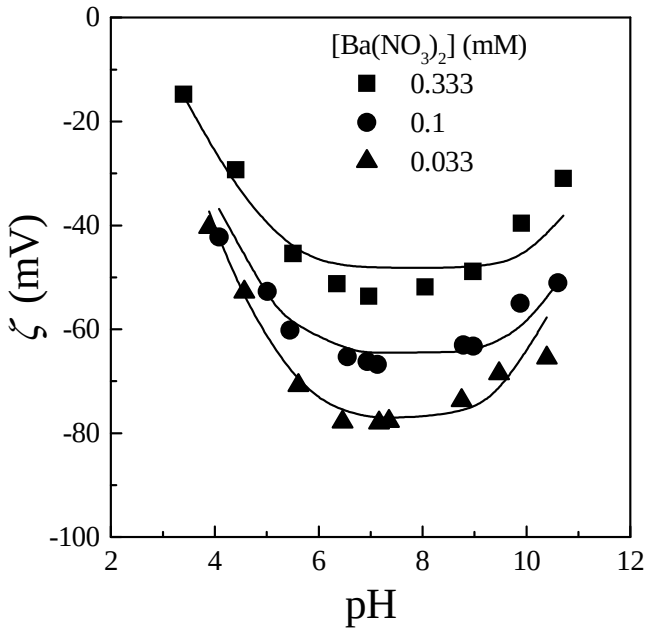

Figure 5

Berli, Piaggio and Deiber, 2002.

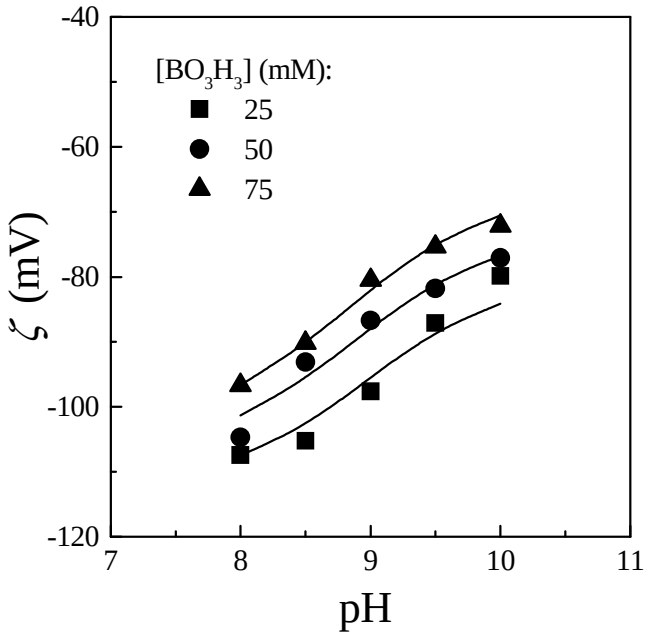

Figure 6

Berli, Piaggio and Deiber, 2002.

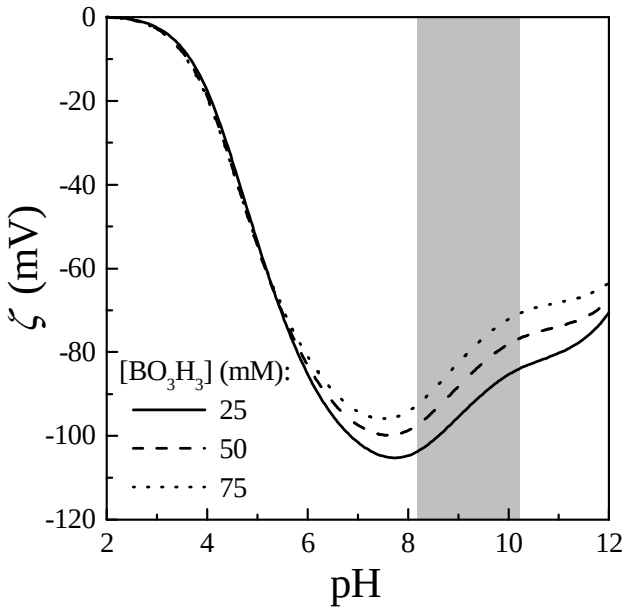

Figure 7

Berli, Piaggio and Deiber, 2002.